Comparison of slip and non-slip mathematical models of AC electroosmosis in microchannels with asymmetric co-planar electrodes

Petr Červenka*, Jiří Hrdlička, Michal Přibyl and Dalimil Šnita

Institute of Chemical Technology, Prague, Department of Chemical Engineering,
Technická 5, 166 28 Praha 6, Czech Republic

* E-mail address: Petr.Cervenka@vscht.cz, Tel.: +420 2 2044 3239, Fax: +420 2 2044 4320

***Abstract*—One type of AC electroosmotic micropumps is driven by a low amplitude AC electric field imposed on systems of co-planar electrodes. Interesting non-linear phenomena such as flow reversals have been observed in experimental studies. The value and the direction of the net velocity depends on the AC electric field parameters, the microchannel geometry and other parameters.**

In this contribution, we present predictions of non-equilibrium and equilibrium mathematical models describing electrolyte transport in these AC micropumps. The classical equilibrium approach is based on the use of the capacitor-resistor boundary conditions for electric potential, the slip boundary conditions for the velocity at electrode surfaces, and the Laplace, the Stokes and the continuity equations. The non-equilibrium mathematical model is based on the mass and momentum balances, the Gauss law, and the non-slip boundary conditions.

We have found that both models predict almost the same behavior of the AC micropumps in low amplitude regimes. If amplitude substantially exceeds the linearization limit ($A \gg 25$mV), the obtained results can qualitatively differ. Parametrical study has revealed that there are „optimal" AC frequency, the vertical confinement of microchannels and the ratio between the size of asymmetric electrodes to attain the maximal time averaged net velocity.

I. Introduction

A design of the AC electrokinetic micropumps was first proposed by Ajdari [1]. The micropump can be constructed by means of arrays of asymmetric pairs of co-planar microelectrodes deposited on a dielectric substrate. It was expected that the asymmetry of the electric field will lead to a net flow of the electrolyte. His predictions were verified by several experimental and theoretical works, e.g., [2–6].

In the co-planar arrangement, the AC electric field imposed on the microelectrodes has the tangential and the normal components. The normal component induces electrode polarization (capacitive charging). Then, the lateral component of the electric field forces the amassed electric charge to move along the electrodes. As the electric charge is formed by ions of a non-zero diameter, the moving ionic particles pull the surrounding liquid via viscous forces. Combination of the coulombic, pressure and viscous forces in a liquid results in the formation of eddies above the electrodes that were experimentally observed by PIV techniques [3, 4]. The system asymmetry leads to an asymmetry of the eddies and finally to a non-zero net velocity.

Mathematical models of AC electroosmosis have been developed. The computation domain is usually divided into the capacitor domains (the electric double layers – EDLs) and the resistor domain (electrolyte bulk). Then, the boundary conditions for electric potential on the capacitor-resistor interfaces can be derived. However, these boundary conditions are valid only when a low voltage (amplitude $< 25\,\mathrm{mV}$) is applied on the microelectrodes, i.e., the linearization of the Poisson-Boltzmann equation is justified [12]. Ones the distribution of the electric potential at the capacitor-resistor interface is evaluated, then velocity slip boundary conditions on the electrode surfaces can be expressed by the Helmholtz-Smoluchowski equation [7]. So, the transport (flow) problem is solved independently only in the resistor domain represented by the electrolyte bulk.

Alternative non-equilibrium models have been developed [10, 13, 14]. This approach allows analyzing the model equations for voltages above the linearization limit (amplitude $\gg 25\,\mathrm{mV}$) with non-equilibrated EDL. The non-equilibrium models describe the distribution of electric potential with the use of the Poisson equation and the molar balances of ions. However, the flow problem has to be solved simultaneously. The Navier-Stokes, the continuity equation and the zero (non-slip) velocity boundary conditions are used.

II. Mathematical model

A. Micropump configuration

The co-planar arrangement of the AC electroosmotic pumps is considered, Fig. 1. The studied microfluidic pump can be represented by a single segment of a long microfluidic channel. We assume that a microchannel consists of an infinitely large series of the segment with periodic boundary conditions. We assume that width of the microchannels is much larger than the characteristic dimensions of the segments, so the AC electroosmotic pumps can be described as two-dimensional

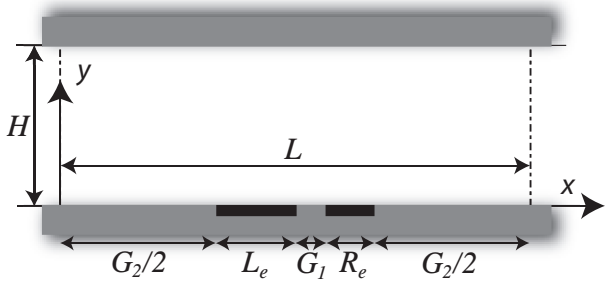

Fig. 1. Scheme of one segment of the AC electroosmotic micropump. Dashed-dotted lines indicate the periodic boundary conditions.

objects of length L and height H. The electrodes have length L_e and R_e and are separated by two gaps G_1, G_2.

A symmetric mono-monovalent water electrolyte (e.g., potassium chloride) is considered as the fluid in microchannels. No changes of density, viscosity and temperature are expected. No faradaic reactions are assumed on the electrodes. Formation of the Stern part of EDL or condensed EDL is not considered in this study.

B. Non-equilibrium approach

The model equations are transformed into a dimensionless form. The spatial coordinates and dimensions the pump and EDL thickness are scaled by the factor L :

$$\tilde{x} = \frac{x}{L}\ ,\quad \tilde{y} = \frac{y}{L}\ ,\quad \tilde{\lambda}_D = \frac{\lambda_D}{L}\,,$$

where the Debye length (λ_D) is defined by

$$\lambda_D^2 = \frac{\varepsilon RT}{2\,c_\circ F^2}\,,$$

The characteristics dimensions were transformed to dimensionless form. The dimensionless height of the channel, the ratio between electrode sizes, the ratio of the gap sizes and the relative ratio of electrode and nonelectrode domains are defined by

$$\tilde{h} = \frac{H}{L}\ ,\quad \tilde{l} = \frac{L_e}{R_e}\ ,\quad \tilde{g} = \frac{G_1}{G_2}\ ,\quad \tilde{l_e} = \frac{L_e + R_e}{L}\,.$$

The dimensionless time $\tilde{t}$ and the frequency $\tilde{f}$ are given by

$$\tilde{t} = \frac{t}{t_\circ}\ ,\quad t_\circ = \frac{\lambda_D L}{D}\ ,\quad \tilde{f} = f t_\circ\,.$$

The other dimensionless quantities are defined by

$$\tilde{q} = \frac{(c^+ - c^-)}{2\,c_\circ}\ ,\quad \tilde{c} = \frac{c^+ + c^-}{2\,c_\circ}\,,$$

$$\tilde{\varphi} = \frac{\varphi}{\varphi_\circ}\ ,\quad \varphi_\circ = \frac{RT}{F}\ ,\quad \tilde{\psi} = \frac{\psi}{\varphi_\circ}\ ,\quad \tilde{A} = \frac{A}{\varphi_\circ}\,,$$

$$\tilde{\mathbf{v}} = \frac{\mathbf{v}}{D/L}\ ,\quad \tilde{p} = \frac{p}{2\,c_\circ RT}\,.$$

The velocity and pressure fields in the electrolyte are described by the Navier-Stokes equation and the continuity equation for an incompressible Newtonian fluid

$$\frac{1}{\mathrm{Sc}}\left(\frac{\partial\tilde{\mathbf{v}}}{\partial\tilde{t}} + \tilde{\lambda}_D\tilde{\mathbf{v}}\cdot\tilde{\nabla}\tilde{\mathbf{v}}\right) =$$

$$= \tilde{\lambda}_D\tilde{\nabla}^2\tilde{\mathbf{v}} + \frac{\mathrm{Ra}}{\tilde{\lambda}_D}\left(-\tilde{\nabla}\tilde{p} - \tilde{q}\tilde{\nabla}\tilde{\varphi}\right)\,, \qquad (1)$$

$$\tilde{\nabla}\cdot\tilde{\mathbf{v}} = 0\,. \qquad (2)$$

where Sc is the Schmidt number and Ra is the Raleygh number defined by

$$\mathrm{Ra} = \frac{\varepsilon}{\eta D}\left(\frac{RT}{F}\right)^2\ ,\quad \mathrm{Sc} = \frac{\eta}{\rho D}\,.$$

The electric potential field satisfies the Poisson equation

$$\tilde{\nabla}^2\tilde{\varphi} = -\tilde{\lambda}_D^{-2}\tilde{q}\,. \qquad (3)$$

In order to evaluate the field of electric charge density, two molar balances for the anion (-) and the cation (+) have to be used. The total molar flux density of an ion is given by the sum of the convective, the electromigration and the diffusion contributions. Linear combinations of two molar balances gives the equations for concentration and conductivity in the dimensionless form.

$$\frac{\partial\tilde{c}}{\partial\tilde{t}} = -\tilde{\lambda}_D\tilde{\nabla}\cdot\left(\tilde{\mathbf{v}}\tilde{c} - \tilde{\nabla}\tilde{c} - \tilde{q}\tilde{\nabla}\tilde{\varphi}\right)\,, \qquad (4)$$

$$\frac{\partial\tilde{q}}{\partial\tilde{t}} = -\tilde{\lambda}_D\tilde{\nabla}\cdot\left(\tilde{\mathbf{v}}\tilde{q} - \tilde{\nabla}\tilde{q} - \tilde{c}\tilde{\nabla}\tilde{\varphi}\right)\,, \qquad (5)$$

The non-slip boundary conditions are used for all electrolyte-solid interfaces

$$\tilde{\mathbf{v}} = 0\,. \qquad (6)$$

Electric potential on the electrodes is given by

$$\tilde{\varphi}_L^e = \tilde{A}sin(2\pi\tilde{f}\tilde{t})\ ,\quad \tilde{\varphi}_R^e = 0\,. \qquad (7)$$

The insulating boundary conditions are used for electric potential on the non-electrode solid boundaries

$$\mathbf{n}\cdot\tilde{\nabla}\tilde{\varphi} = 0\,. \qquad (8)$$

The spatially periodical solution is considered

$$\tilde{\xi}(x,y,t) = \tilde{\xi}(x+L,y,t)\ ,\quad \tilde{\xi} = \tilde{\varphi},\tilde{\mathbf{v}},\tilde{p},\tilde{c}^{\pm}\,, \qquad (9)$$

and thus the periodical boundary conditions at $x = 0$ and $x = L$ are applied.

C. Equilibrium approach

The equilibrium approach enables to decouple the electrostatic and the flow parts of the problem. The model equations are transformed into a dimensionless form with the use of same scaling factors as in previous section.

Electrical problem in electrolyte bulk is governed by Laplace equation due to assumption of electroneutrality in the electrolyte bulk

$$\tilde{\nabla}^2 \tilde{\varphi} = 0\,, \tag{10}$$

The boundary conditions for electric potential are the same as in the non-equilibrium model except the electrode boundaries. Here the capacitor-resistor boundary conditions are used [15, 16]

$$\mathbf{n}\cdot\nabla\tilde{\varphi} = -\frac{\partial}{\partial\tilde{t}}\left(\tilde{\varphi}^e - \tilde{\varphi}\right) \tag{11}$$

Using complex formulation

$$\tilde{\varphi}(x,y,t) = \Re\left[\tilde{\psi}(x,y)\,\exp(i2\pi\tilde{f}\tilde{t})\right]\,, \tag{12}$$

where $\tilde{\psi}$ is a complex function expressing the time-independent part of the potential field. We can rewrite equations (10) and (11) in to the form:

$$\tilde{\nabla}^2\tilde{\psi} = 0\,, \tag{13}$$

$$\mathbf{n}\cdot\tilde{\nabla}\tilde{\psi} = -2\pi i\tilde{f}\left(\tilde{\psi}^e - \tilde{\psi}\right)\,, \tag{14}$$

where the difference between electrodes is defined by

$$\tilde{\psi}^e_L = \tilde{A}\exp(-2\pi i\tilde{f}\tilde{t})\,,\quad \tilde{\psi}^e_R = 0\,.$$

The Helmholtz-Smoluchowski equation describes slip velocity on the outer boundary of EDL above the electrodes

$$\tilde{v}_{\mathrm{slip},n} = \mathrm{Ra}\left(\tilde{\varphi}^e_n - \tilde{\varphi}\right)\mathbf{t}\cdot\tilde{\nabla}\tilde{\varphi} =$$

$$= \mathrm{Ra}\Re\left[\left(\tilde{\psi}^e_n - \tilde{\psi}\right)\exp(2\pi i\tilde{f}\tilde{t})\right]\mathbf{t}\cdot\Re\left(\tilde{\nabla}\tilde{\psi}\exp(2\pi i\tilde{f}\tilde{t})\right)\,,$$

$$n = R, L\,. \tag{15}$$

The slip velocity represent the tangential velocity at EDL. The normal component of the velocity vector is considered to be zero at EDL.

The time averaged slip velocity averaged over one period of the AC signal is

$$\begin{aligned}\langle\tilde{v}\rangle_{\mathrm{slip},n} &= \frac{\mathrm{Ra}}{2}\Re(\tilde{\psi}^e_n - \tilde{\psi})\mathbf{t}\cdot\Re(\tilde{\nabla}\tilde{\psi}) \\ &+ \frac{\mathrm{Ra}}{2}\Im(\tilde{\psi}^e_n - \tilde{\psi})\mathbf{t}\cdot\Im(\tilde{\nabla}\tilde{\psi})\,,\quad n = R, L\end{aligned} \tag{16}$$

The time averaged Stokes equation and the continuity equation are then used for description of the bulk hydrodynamics

$$0 = \tilde{\lambda}_D^2\tilde{\nabla}^2\langle\tilde{\mathbf{v}}\rangle - \tilde{\nabla}\langle\tilde{p}\rangle\,,\quad \tilde{\nabla}\cdot\langle\tilde{\mathbf{v}}\rangle = 0\,, \tag{17}$$

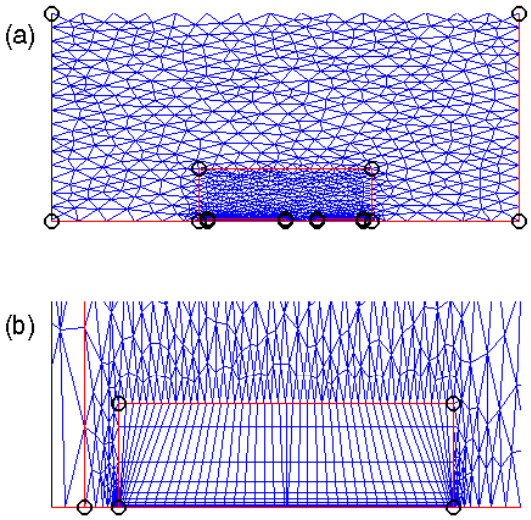

Fig. 2. The discretization mesh consisting of 4100 elements (a) the entire spatial domain (b) the detail above an electrode

III. Numerical analysis

Numerical analyses both of the non-equilibrium and the equilibrium models were carried out in the Comsol Multiphysics software.

We used the standard *femtime* procedure for the dynamical analysis of the non-equilibrium mathematical model, eqs. (1–5) and the boundary conditions (6–9). Transient simulations from a homogeneous steady state to stable periodic regimes were carried out in the first step. The obtained stable periodic solutions were then studied to obtain the time-averaged net velocity and other characteristics of the AC electroosmotic flow.

Analysis of the equilibrium model (13, 17) with boundary conditions (14, 16) was realized in two steps. The analysis of the linear electric potential problem (13) with the boundary condition (14) was done using the *femlin* solver. The flow problem (17) with the boundary condition (16) was then solved by the *femnlin* solver.

The Comsol Multiphysics software requires discretization of the spatial computation domain into a set of finite elements. For the non-equilibrium model, we used hybrid triangle-rectangle meshes of finite elements that enable efficient discretization the entire spatial domain including the electrical double layers. The equilibrium model requires only the discretization using triangle finite elements with a higher density at the electrode edges, Fig 2.

IV. Results

In order to estimate numerical errors resulting from the spatial discretization of the computational domain, we used meshes with various spatial density for the analysis of the non-equilibrium model. Several comparisons of results obtained by means of different meshes are presented. Dependencies of the dimensionless time averaged net velocity on the dimensionless frequency and amplitude of AC electric field and on the ratio

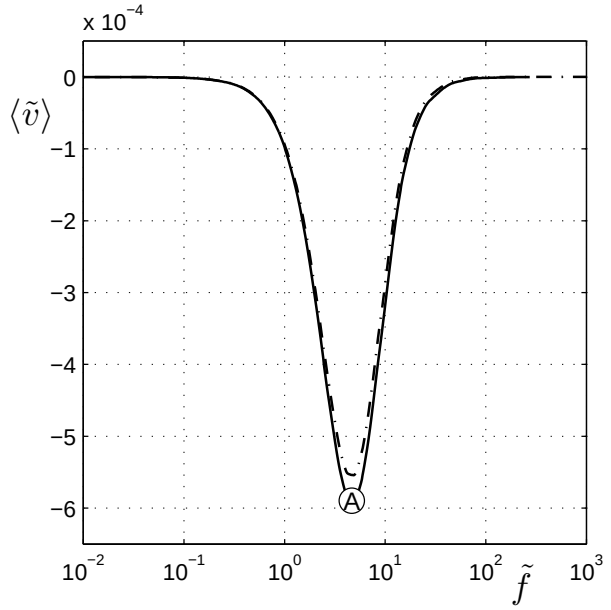

Fig. 3. Dependencies of the time averaged net velocity on the AC frequency, the equilibrium model - dash-dotted lines, the non-equilibrium model - solid lines, $\tilde{h} = 0.333$, $\tilde{l} = 1.667$, $\tilde{\lambda}_D = 3.3 \times 10^{-3}$, $\tilde{A} = 0.75$

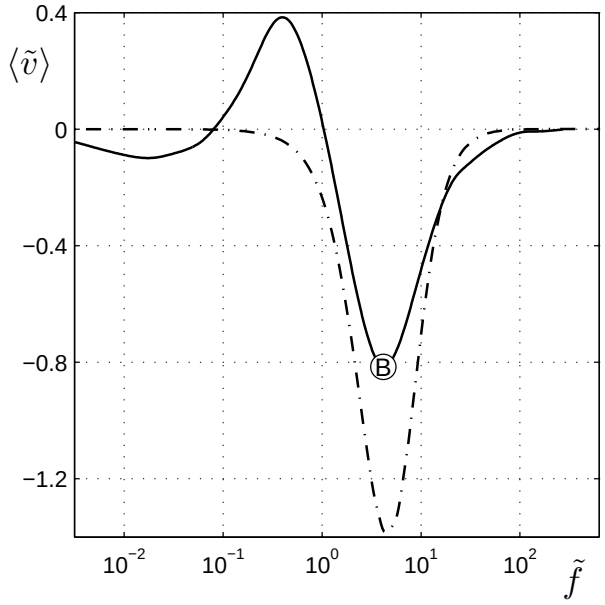

Fig. 4. Dependencies of the time averaged net velocity on the AC frequency, the equilibrium model - dash-dotted lines, the non-equilibrium model - solid lines, $\tilde{h} = 0.333$, $\tilde{l} = 1.667$, $\tilde{\lambda}_D = 3.3 \times 10^{-3}$, $\tilde{A} = 37.4$

between electrode dimensions and on the microchannel height were computed. The results obtained from analyses of the equilibrium (dash-dotted lines) and the non-equilibrium (solid lines) models are compared. The detected discrepancies and their possible origins are discussed.

A. Frequency characteristics

The dependencies of the dimensionless time averaged net velocity on the dimensionless frequency of electric field are presented in Figs. 3-5. All velocity maxima (in the absolute value) are located around $\tilde{f} = 1$. It agrees with the prediction of the RC circuit theory for the AC electroosmotic systems [12]. It should be noted that the precise location on the frequency characteristics, depends on the particular choice of the characteristic length. In this paper, the length of periodic domain is chosen to be the characteristic length. For low amplitude regime, the results are in a qualitative and almost in a quantitative agreement, Fig 3. The dependency has single maximum and the flow reversal is not predicted. The relative deviations between predictions of the analyzed models are less than 15% in the entire frequency range. This result can be expected because the linearization used in the equilibrium model is justified for the system where $\tilde{A} < 1$. The deviation can be caused by numerical erorrs and the limitations of the equilibrium model (1D character of EDL, effect of the vertical dimension of the model domain etc.)

The velocity dependencies for the dimensionless amplitude $\tilde{A} = 37.4$ are depicted in Figs. 4, 5. Two regimes with different $\tilde{\lambda}_D$ were chosen. Both the dependencies has a nonlinear shape. The equilibrium model predicts a single velocity maximum of the frequency characteristics. In the first regime ($\tilde{\lambda}_D = 3.3 \times 10^{-3}$,Fig. 4), flow reversal is observed on the non-equilibrium characteristics. The velocity maxima (in the absolute value) for both the models are located at the same frequency, however, the equilibrium model predicts higher time averaged net velocity (The relative difference is about 50%). In the latter regime($\tilde{\lambda}_D = 3.3 \times 10^{-2}$,Fig. 5), the

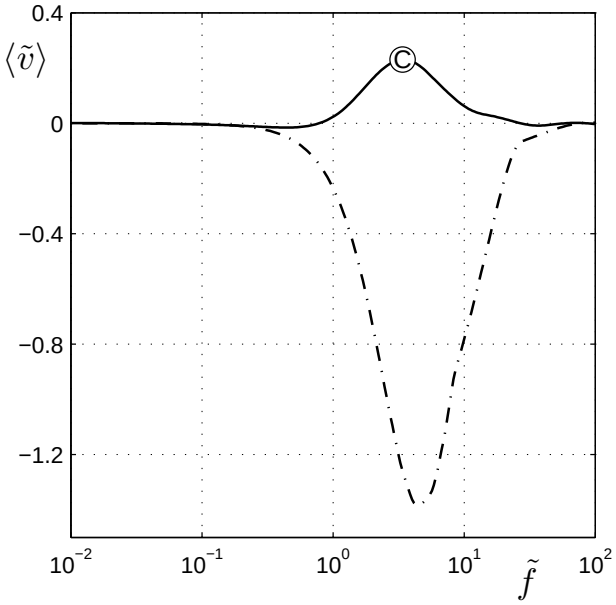

Fig. 5. Dependencies of the time averaged net velocity on the AC frequency, the equilibrium model - dash-dotted lines, the non-equilibrium model - solid lines, $\tilde{h} = 0.333$, $\tilde{l} = 1.667$, $\tilde{\lambda}_D = 3.3 \times 10^{-2}$, $\tilde{A} = 37.4$

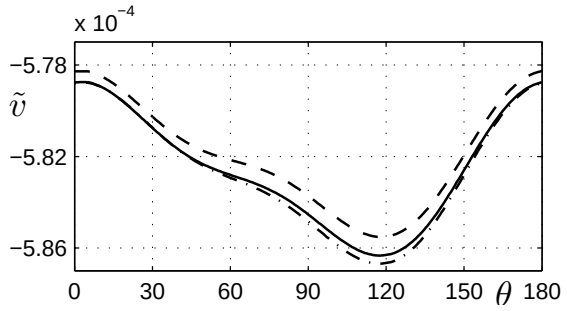

Fig. 6. Dependence of net velocity on the phase of electric field during one half of a period for three different meshes, dashed line - 2100 elements, dash-dotted line - 4100 elements, solid lines - 9000 elements, $\tilde{h} = 0.333$, $\tilde{l} = 1.667$, $\tilde{\lambda}_D = 3.3 \times 10^{-3}$, $\tilde{A} = 0.75$, $\tilde{f} = 3$

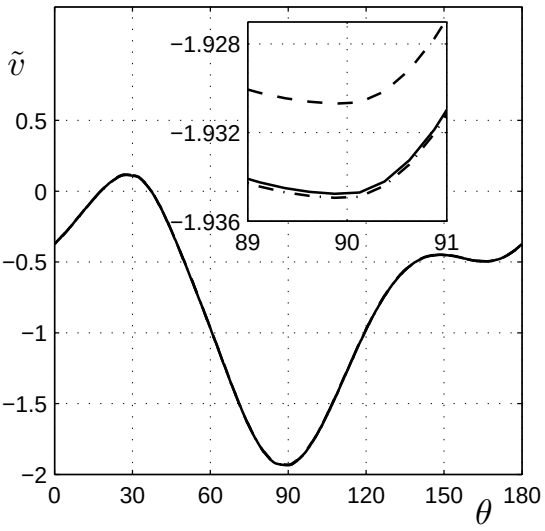

Fig. 7. Dependence of net velocity on the phase of electric field during one half of a period for three different meshes, dashed line - 2100 elements, dash-dotted line - 4100 elements, solid lines - 9000 elements, $\tilde{h} = 0.333$, $\tilde{l} = 1.667$, $\tilde{\lambda}_D = 3.3 \times 10^{-3}$, $\tilde{A} = 37.4$, $\tilde{f} = 3$

frequency dependencies have completely different qualitative character. The net flow obtained from the equilibrium model has even the opposite direction than that given by the non-equilibrium model. In a high amplitude regimes, the results predicted by the equilibrium model must be then strongly deviated from the real behavior. Possible numerical errors can negatively affect especially the non-equilibrium results.

B. Meshtests

As an improper spatial discretization can result in an unacceptable error of the numerical approximation, meshes of various structures and densities were tested. Three sets of model parameters corresponding to symbols A, B, C marked on the frequency dependencies in Figs. 3-5 were chosen for testing of mesh quality. The numerical errors of the results obtained from non-equilibrium model are evaluated in this section. The time dependencies of the net velocity on the phase of electric field θ during one half of a period are depicted in

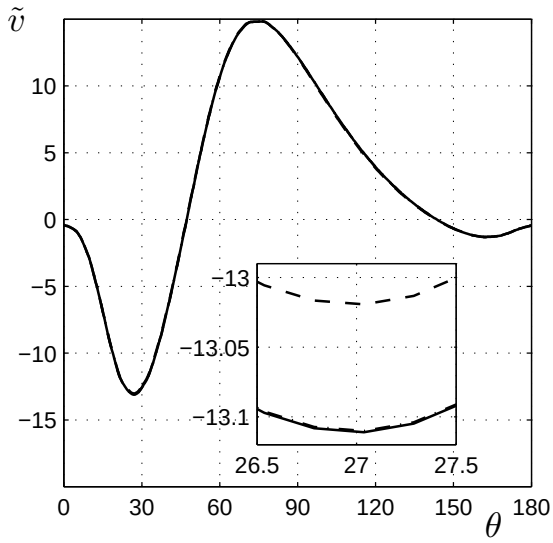

Fig. 8. Dependence of net velocity on the phase of electric field during one half of a period for three different meshes, dashed line - 2100 elements, dash-dotted line - 4100 elements, solid lines - 9000 elements, $\tilde{h} = 0.333$, $\tilde{l} = 1.667$, $\tilde{\lambda}_D = 3.3 \times 10^{-2}$, $\tilde{A} = 37.4$, $\tilde{f} = 3$

Figs. 6-8. Three different meshes are tested (2100, 4100 and 9000 elements). The mesh consisting of 4100 elements with detail above electrode is shown in Fig. 2. For low amplitude regime in Fig. 6 the relative errors of net velocity caused by the spatial disretization are less than 1%. It can be seen that the relative errors of net velocity for high amplitude regimes, Figs. 7, 8, are also less than 1%. Although, the quality of used meshes seems to be good enough, numerical errors can also results from an improper settings of the time solver or the data postprocessing. These factors will be further studied.

C. Amplitude characteristics

One can expect that both the models produce similar results when the amplitude will not substantially exceed the linearization limit ($\tilde{A} = 1$). Thus the velocity dependencies on the amplitude of the applied electric signal were computed, Figs. 9, 10. According to the theory [17], the velocity predicted by the equilibrium model is proportional to the amplitude square. The same is true for the non-equilibrium model up to $\tilde{A} \approx 4$. The non-equilibrium dependencies become nonlinear for higher amplitudes. The flow reversal on the amplitude characteristics is observed for the non-equilibrium model at $\tilde{A} \sim 30$, Fig. 9.

D. Microchannel height

Dependencies of the dimensionless time averaged net velocity on the microchannel height are plotted in Figs. 11, 12. Zero velocity is expected for very thin microchannels due to a negligible electrode polarization. There are clear maxima of the time averaged net velocity (in the absolute value) on the computed dependencies. Micropumps with a larger vertical dimension are not affected by the top solid boundary and the time averaged net velocity approaches an asymptotic value.

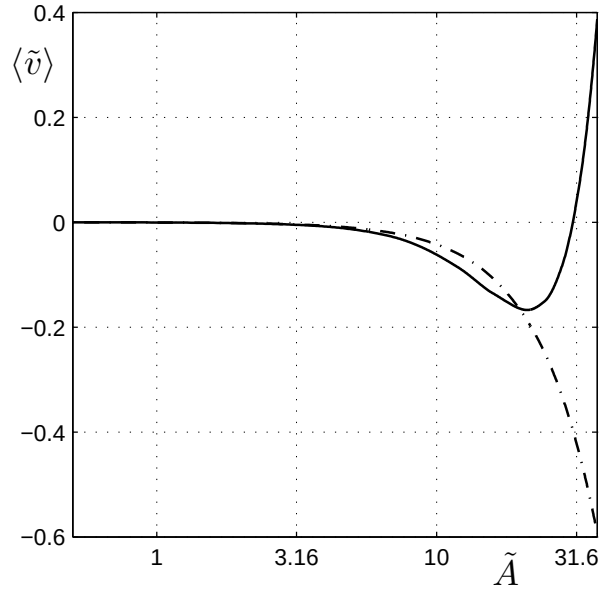

Fig. 9. Dependencies of the time averaged net velocity on the AC amplitude, the equilibrium model - dash-dotted lines, the non-equilibrium model - solid lines, $\tilde{h} = 0.333$, $\tilde{l} = 1.667$, $\tilde{\lambda}_D = 1 \times 10^{-2}$, $\tilde{f} = 0.95$

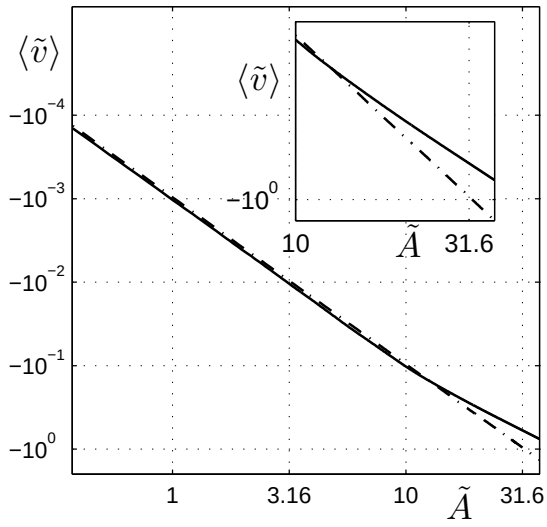

Fig. 10. Dependencies of the time averaged net velocity on the AC amplitude, the equilibrium model - dash-dotted lines, the non-equilibrium model - solid lines, $\tilde{h} = 0.333$, $\tilde{l} = 1.667$, $\tilde{\lambda}_D = 3.3 \times 10^{-3}$, $\tilde{f} = 3$

In low amplitude regimes, Fig. 11, the predictions given by both the models are very similar. In a high amplitude regime, Fig. 12, the time averaged net velocity computed by the non-equilibrium model is smaller (in the absolute value) than that given by the equilibrium model for any vertical extent of the channel. It must be noted that the equilibrium model can not correctly predict the behavior of the pump if the Debye length is comparable with microchannel height. The presence of the non-monotonous part of the non-equilibrium dependence will be further verified.

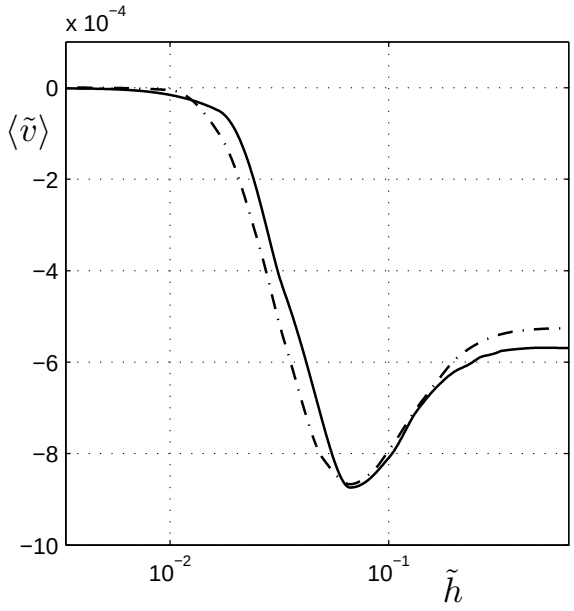

Fig. 11. Dependencies of the time averaged net velocity on the microchannel height, the equilibrium model - dash-dotted lines, the non-equilibrium model - solid lines, $\tilde{l} = 1.667$, $\tilde{\lambda}_D = 3.3 \times 10^{-3}$, $\tilde{f} = 3$, $\tilde{A} = 0.75$

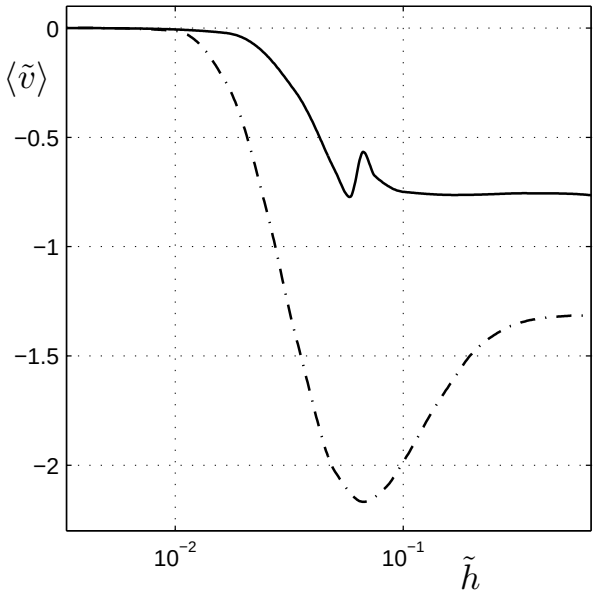

Fig. 12. Dependencies of the time averaged net velocity on the microchannel height, the equilibrium model - dash-dotted lines, the non-equilibrium model - solid lines, $\tilde{l} = 1.667$, $\tilde{\lambda}_D = 3.3 \times 10^{-3}$, $\tilde{f} = 3$, $\tilde{A} = 37.4$

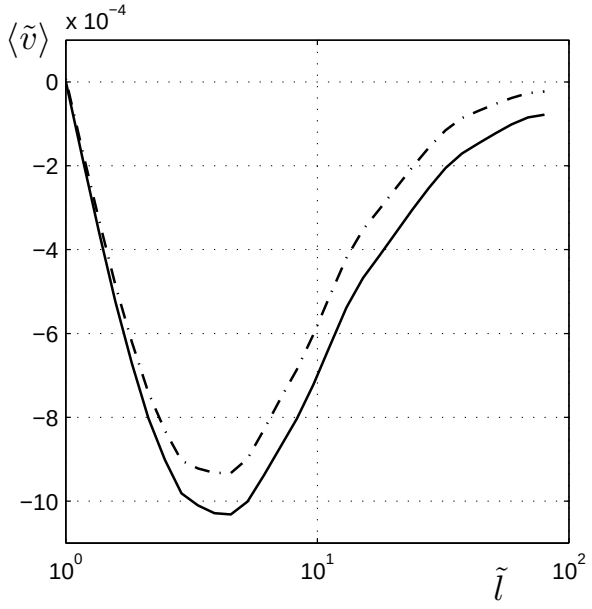

Fig. 13. Dependencies of the time averaged net velocity on the electrode length ratio, the equilibrium model - dash-dotted lines, the non-equilibrium model - solid lines, $\tilde{h} = 0.333$, $\tilde{\lambda}_D = 3.3 \times 10^{-3}$, $\tilde{f} = 3$, $\tilde{A} = 0.75$

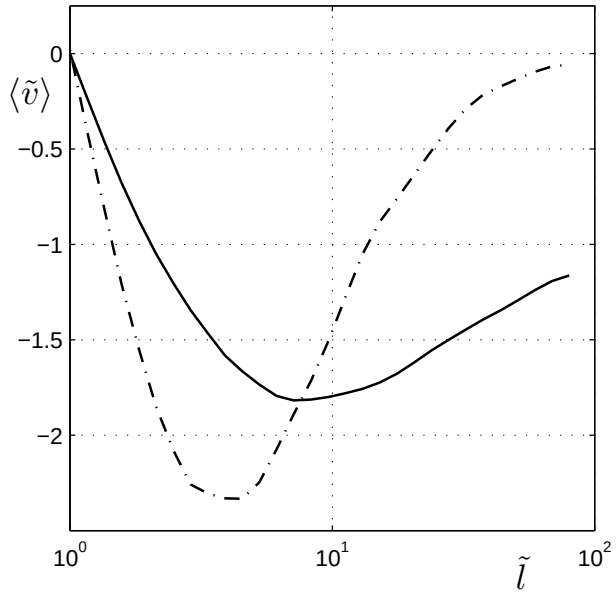

Fig. 14. Dependencies of the time averaged net velocity on the electrode length ratio, the equilibrium model - dash-dotted lines, the non-equilibrium model - solid lines, $\tilde{h} = 0.333$, $\tilde{\lambda}_D = 3.3 \times 10^{-3}$, $\tilde{f} = 3$, $\tilde{A} = 37.4$

E. Electrode size ratio

When the AC electroosmotic micropumps are constructed, the size ratio between the larger and the smaller electrodes can be crucial for their performance. We have found that there is a value of the ratio that enables to attain the maximal time averaged net velocity, Figs. 13, 14. In low amplitude regimes, Fig. 13, the predicted velocity dependencies almost coincide and the maximal time averaged net velocity (in the absolute value) is located at $\tilde{l} = 4$. Substantial quantitative differences are observed in high amplitude regimes, Fig. 14. Location of the velocity maximum (in the absolute value) is $\tilde{l} = 4$ for the equilibrium model and $\tilde{l} = 7.1$ for the non-equilibrium model. Moreover, the non-equilibrium dependence reveals smaller sensitivity with respect to the choice of the electrode size ratio.

V. Conclusion

Dependencies of the time averaged net velocity on principal model parameters for the proposed AC electroosmotic pump with asymmetric electrodes in the coplanar arrangement were obtained. Two different mathematical models were numerically analyzed. It was found that there are „optimal“ sets of model parameters (the electrode size ratio, the vertical dimension of the micropump, the AC frequency) to obtain the maximal pumping velocity. Predictions of these models are similar only in low amplitude regimes. In principle, the non-equilibrium model should be able to analyze the behavior of the micropump in a substantially larger parametric space. However, the obtained result can suffer from numerical artifacts. In future, we plan to verify the obtained results by both an improved numerical code and physical experiments.

Acknowledgment

The authors would like to thank for the support by the grant of the GAAV ČR (KAN208240651), by the grant of the MŠMT ČR (MSM 6046137306), and by the grant GAČR (GD 104/08/H055).

List of symbols

A	amplitude [V]
c	concentration [molm^{-3}]
D	diffusivity [m^2 s^{-1}]
f	frequency [s^{-1}]
F	the Faraday constant [Cmol^{-1}]
H	microchannel height [m]
L	length of a periodic segment [m]
$\mathbf{n}$	normal unit vector
p	pressure [Pa]
R	molar gas constant [JK^{-1}mol^{-1}]
t	time [s]
$\mathbf{t}$	tangential unit vector
T	temperature [K]
v_{slip}	slip velocity [ms^{-1}]
$\langle v \rangle_{slip}$	time averaged slip velocity [ms^{-1}]
v	net velocity [ms^{-1}]
$\langle v \rangle$	time averaged net velocity [ms^{-1}]
$\mathbf{v}$	velocity [ms^{-1}]
x	spatial coordinate [m]
y	spatial coordinate [m]

Greek symbols

ε	electrolyte permittivity [Fm^{-1}]

φ	electric potential [V]
η	dynamic viscosity [Pas]
λ_D	the Debye length [m]
ψ	complex electric potential [V]
ρ	density [kgm^{-3}]
θ	phase of electric field [deg]

Superscripts

e	electrode
$\sim$	dimensionless
$-$	anion
$+$	cation
$\pm$	either $^+$ or $^-$

Subscripts

$\circ$	characteristic value
R	right electrode
L	left electrode

Dimensionless parameters

$\tilde{g}$	the ratio of the gap sizes	$\tilde{g} = 0.1$
$\tilde{l}_e$	ratio of electrode and nonelectrode domains	$\tilde{l}_e = 0.2667$
Ra	Raleygh number	$\mathrm{Ra} = 0.372$
Sc	Schmidt number	$\mathrm{Sc} = 348$

REFERENCES

[1] Ajdari A (2000), Physical Review E 61:R45

[2] Campisi M, Accoto D, Dario P (2005), Journal of Chemical Physics 123:204724

[3] Garcia-Sanchez P, Ramos A, Green G *et. al.* (2006), IEEE Transactions on Dielectrics and Electrical Insulation 13:670

[4] Green N G, Ramos A, Gonzalez A *et. al.* (2002), Physical Review E 66:026305

[5] Mpholo M, Smith C G, Brown A B D (2003), Sensors and Actuators B-Chemical 92:262

[6] Studer V, Pepin A, Chen Y *et. al.* (2004), Analyst 129:944

[7] *Physicochemical hydrodynamics: An Introduction*, Wiley and Sons, New York, 1994.

[8] Green N G, Ramos A, Morgan H (2000), Journal of Physics D-Applied Physics 33:632

[9] Urbanski J P, Levitan J A, Burch D N *et. al.* (2007), Journal of Colloid and Interface Science 309:332

[10] Mortensen N A, Olesen L H, Belmon L *et. al.* (2005), Physical Review E 71:056306

[11] Ramos A, Morgan H, Green N G *et. al.* (2005), Journal of Applied Physics 97:084906

[12] Squires T M, Bazant M Z (2004), Journal of Fluid Mechanics 509:217

[13] *Multiphysical Modeling of DC and AC Electroosmosis in Micro- and Nanosystems in Recent Advances in Modelling and Simulation*, Petrone G, Cammarata G, I-Tech Education and Publishing, Vienna, 2008.

[14] Cervenka P, Pribyl M, Snita D (2009, In press), Microelectronic engineering

[15] Levitan J A, Devasenathipathy S, Studer V *et. al.* (2005), Colloids and Surfaces a-Physicochemical and Engineering Aspects 267:122

[16] Gonzlez A, Ramos A, Green N G *et. al.* (2000), Physical Review E 61:4019

[17] Ramos A, Morgan H, Green N G *et. al.* (1998), Journal of Physics D-Applied Physics 31:2338